




cambridge.org/mrf

Pengpeng Chen<sup>1</sup> , Wenjian Wang<sup>1,2</sup>, Lihui Wang<sup>1</sup>, Qihua Lin<sup>1</sup>, Da Hou<sup>1,3</sup> and Zhiyong Luo<sup>1,3</sup>

<sup>1</sup>School of Electronics and Communication Engineering, Sun Yat-sen University, Shenzhen, China; <sup>2</sup>Kuang-Chi Institute of Advanced Technology, Shenzhen, China and <sup>3</sup>Pengcheng Laboratory, Shenzhen, China

## Research Paper

**Cite this article:** Chen P, Wang W, Wang L, Lin Q, Hou D, Luo Z (2024) A compact wideband high-gain circularly polarized array antenna based on SIGW-SRP. *International Journal of Microwave and Wireless Technologies*, 1–12. <https://doi.org/10.1017/S175907872400134X>

Received: 20 June 2024  
Revised: 3 December 2024  
Accepted: 5 December 2024

### Keywords:

circularly polarized antenna;  
substrate integrated gap waveguide;  
wideband antenna

**Corresponding author:** Zhiyong Luo;  
Email: [luozhy57@mail.sysu.edu.cn](mailto:luozhy57@mail.sysu.edu.cn)

### Abstract

A compact, wideband, and high-gain circularly polarized array antenna is proposed based on substrate integrated gap waveguide (SIGW) using sequential rotational phase (SRP). The array antenna consists of four  $2 \times 2$  corner-cutting corner patches and an SIGW-SRP feeding network. The SIGW-SRP feeding network is achieved by utilizing the spatial vector addition property to compensate for phase, aiming to improve the bandwidth and gain. Unlike the traditional SRP feeding network, the proposed feeding scheme is simpler and easier to fabricate, and each port can achieve more stable phase and bandwidth. In addition, benefiting from the surface wave suppression and in-phase reflection property of SIGW, the proposed array antenna has a stable radiation pattern and low cross-polarization covering wideband frequencies. The measured results indicate that the  $-10$ -dB impedance bandwidth ranges from 12.2 to 17.3 GHz (34.6%), the 3-dB axial ratio bandwidth ranges from 13.5 to 16.7 GHz (21.2%), and the peak gain is 16 dBic.

## Introduction

Antenna serves an important part of the communication system, and its performance directly affects the quality and reliability of communication. Circularly polarized (CP) antennas have strong anti-interference ability and good anti-multipath fading performance, providing stable and reliable communication services in complex communication environments [1–3].

At present, there are many methods to achieve circular polarization, which are mainly divided into single-point feeding [4, 5] and multi-point feeding [6, 7]. Specifically, in order to improve the axial ratio bandwidth (ARBW), several methods have been proposed, such as the use of multilayer structure [8, 9], metasurface antenna with periodic structure [10, 11], and the use of sequential rotation phase (SRP) feeding network [12, 13]. The multilayer structure improves the bandwidth by introducing additional resonant properties. In [14], a double-layer radiating patch is proposed, where the lower patch consists of a square outer loop and a three-quarter ring inner loop, and the upper layer is used for impedance matching, achieving a  $-10$ -dB impedance bandwidth (IBW) of 15.2% and a 3-dB ARBW of 8.2%, as well as a peak gain of 7 dBi. Metasurface antenna achieves bandwidth expansion by changing the surface impedance distribution by adjusting the size, shape, and arrangement of the periodic elements. In [15], a low-profile coplanar waveguide metasurface antenna is proposed, which is excited by a coplanar waveguide (CPW) feeding with a certain rotation angle at the bottom, and achieves a  $-10$ -dB IBW of 25%, a 3-dB ARBW of 19%, and a peak gain of 8 dBi. Compared with the previous two methods, the CP array antenna implemented by SRP technology can improve CP characteristics by introducing phase differences between different subarrays [16], it is easier to achieve higher gain and wider bandwidth. In [17], a wideband CP antenna array is proposed based on SRP using crossed-dipole elements, achieving a  $-10$ -dB IBW of 44%, a 3-dB ARBW of 34.6%, a peak gain of 11 dBic, and its overall size is  $1.89\lambda_0 \times 1.65\lambda_0 \times 0.11\lambda_0$ . In [18], a substrate integrated waveguide cavity antenna array based on metasurface is achieved, with a  $-10$ -dB IBW of 38%, a 3-dB ARBW of 24.9%, a peak gain of 12.1 dBic, and an overall size of  $2.18\lambda_0 \times 2.18\lambda_0 \times 0.06\lambda_0$ . However, array antennas based on SRP generally suffer from the issues of large design size and low gain, which is not suitable for the current development trend of communication systems. Additionally, for space-limited scenarios, such as satellite communications, achieving high gain and high polarization purity (low cross-polarization) remains a challenge.

To solve the above issues, a compact wideband and high-gain  $2 \times 2$  CP array antenna is achieved using SRP feeding network based on substrate integrated gap waveguide (SIGW). SIGW is a novel waveguide structure that has been proposed in recent years [19, 20]. It merits

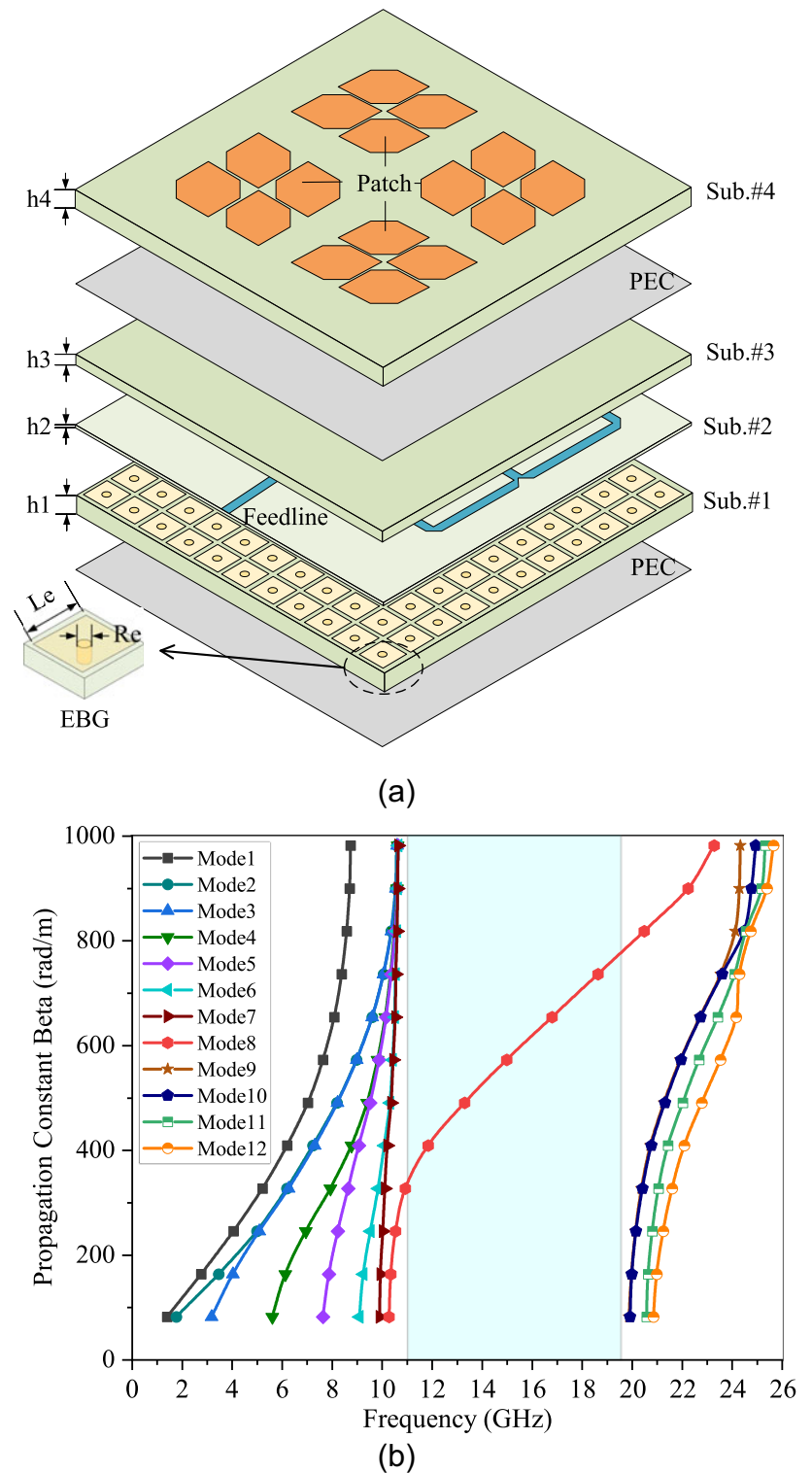


**Figure 1.** (a) Structure of the array antenna. (b) SIGW dispersion curve. The relevant parameters are:  $h1 = 0.813$ ,  $h2 = 0.203$ ,  $h3 = 0.508$ ,  $h4 = 0.813$ ,  $Le = 2.4$ ,  $Re = 0.3$  (units: mm).

advantages such as low radiation loss and easy integration, making it widely used in the design of various microwave devices, such as filters [21] and antennas [22]. Compared to traditional SRP feeding network, the SIGW-SRP feeding network structure proposed in this paper is simple, easy to fabricate, and enables to achieve compact array antenna. The final implemented wideband high-gain CP array antenna has low cross polarization and low back radiation,

and achieves  $-10$ -dB IBW of 34.6%, 3-dB ARBW of 21.2%, and the peak gain of 16 dBic. The overall size is only  $1.5\lambda_0 \times 1.5\lambda_0 \times 0.11\lambda_0$ .

Section 2 presents the structure and operating mechanism of the proposed array antenna, including the antenna element and the SIGW-SRP feeding network. Section 3 provides the measured results of the proposed array antenna and some brief discussions. Finally, Section 4 presents the conclusions.

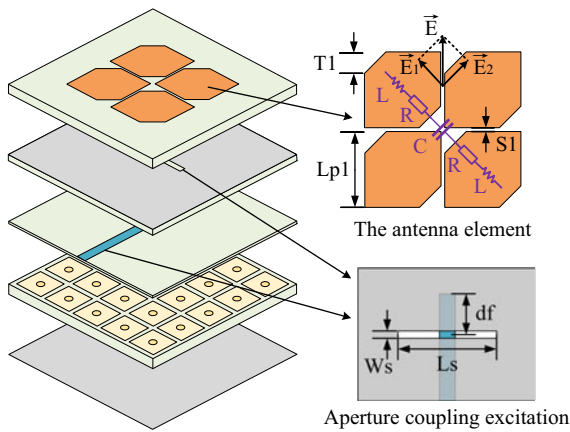


**Figure 2.** The overall structure of the antenna element. The relevant parameters of the proposed antenna element are:  $T1 = 1.2$ ,  $Lp1 = 4.2$ ,  $S1 = 0.2$ ,  $df = 1.8$ ,  $Ls = 6$ ,  $Ws = 0.5$  (units: mm).

### Feed network structure design based on SIGW-SRP

#### Array antenna structure design

As shown in Fig. 1(a), the proposed array antenna is composed of four layers of dielectric substrates, and all substrate materials are Rogers 4003C ( $\epsilon_r = 3.55$  and  $\tan \delta = 0.0027$ ). Sub.#1 to Sub.#3 form SIGW structure (Sub.#1 consists of periodic Electromagnetic Band Gap (EBG) cells, Sub.#2 serves as an isolation layer, and the upper surface of Sub.#3 is printed perfect electric conductor (PEC) as GND). Furthermore, the dispersion curve of SIGW is shown in Fig. 1(b). It can be observed that the electromagnetic bandgap range is 11–19.5 GHz, and only one Quasi-Transverse Electromagnetic Mode (Quasi-TEM) wave can propagate within the bandgap, which means minimum distortion during signal transmission. In addition, the array antenna consists of four  $2 \times 2$  corner-cutting patch elements placed orthogonally (achieving stable and symmetry radiation patterns).

In SIGW, since the electric field is almost confined to the region between the inner microstripline (MSL) and the upper PEC [23], then when all dielectric substrates of SIGW have the same material, SIGW can be approximated as the MSL with the relative permittivity  $\epsilon_r$  filled by the surrounding dielectric. In this way, the characteristic impedance of SIGW can be approximately calculated using the characteristic impedance of MSL [16]:

$$Z_{SIGW} \cong \sqrt{\frac{\epsilon_e}{\epsilon_r}} Z_{MSL} \quad (1)$$

where  $Z_{MSL}$  is the characteristic impedance of MSL,  $Z_{SIGW}$  is the characteristic impedance of SIGW, and  $\epsilon_e$  is the effective permittivity. The use of SIGW benefits the suppression of cross polarization and back lobe radiation, and contributes to improve the forward radiation of the array antenna [22].

#### Antenna element design and analysis

The antenna element structure is shown in Fig. 2, and the CP radiation performance can be explained by the equivalent circuit. The electric field  $\vec{E}$  generated by the antenna element is decomposed into two orthogonal components  $\vec{E}_1$  and  $\vec{E}_2$ . The equivalent impedances on  $\vec{E}_1$  and  $\vec{E}_2$  directions are not equal because of the perturbation caused by the exist of the corner-cutting on the antenna element [24]:

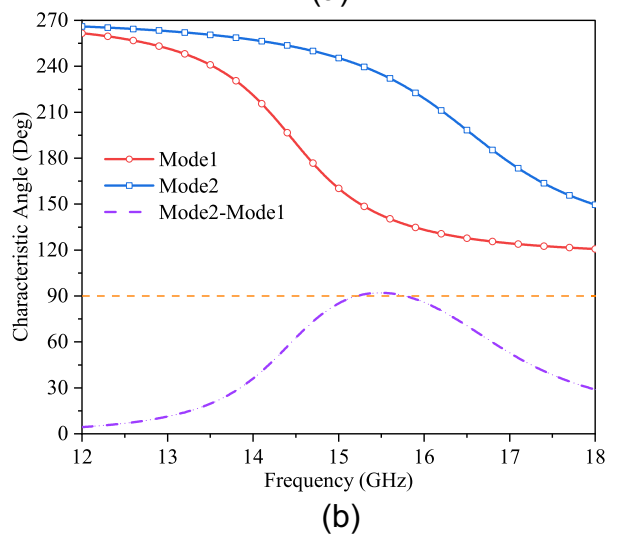
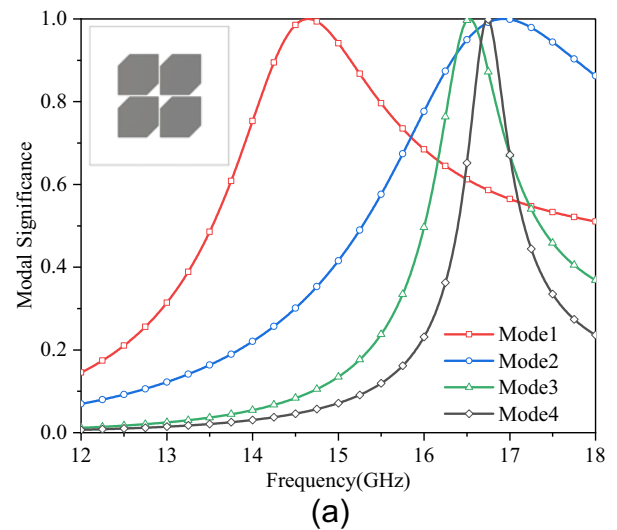


**Figure 3.** (a) MS of the first two modes. (b) CA of the first two modes.

$$Z_i = R_i + jX_i = 2R_i + j\omega(2L_i) + \frac{1}{j\omega C_i} \quad (2)$$

where  $R_i$  is the resistance of the patch,  $L_i$  is the inductance generated from the patch to GND, and  $C_i$  is the capacitance due to the gap between diagonal patches ( $i = 1, 2$ ). When  $X_i = 0$ , the antenna resonates and the resonant frequency can be obtained, where  $X_i = 0$  is the reactance. Since the corner-cutting increases the gap of the diagonal patches, it will change the impedance value. When the size of  $T1$  is set appropriately, the circular polarization condition can be satisfied, and the relationship between the two electric field components is:

$$|\vec{E}_1| = |\vec{E}_2|, \angle \vec{E}_2 - \angle \vec{E}_1 = 90^\circ. \quad (3)$$

When the operating wavelength is given, a wide circular polarization with good axial ratio can be achieved by selecting appropriate antenna dimensions and the relative permittivity of the substrate. For a single corner-cutting patch, the calculation formula for the size of the corner-cutting is as follows:

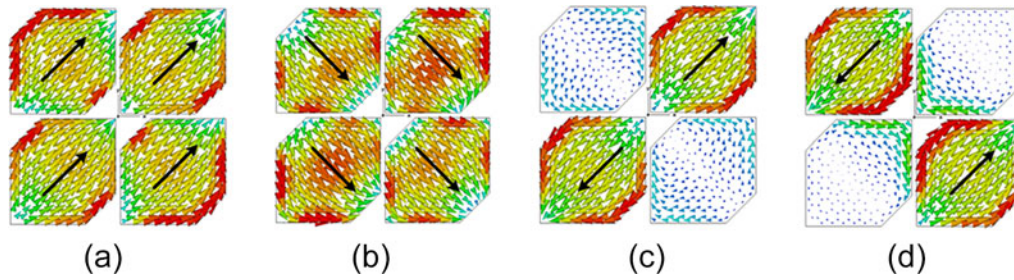


Figure 4. Surface current. (a) Mode1. (b) Mode2. (c) Mode3. (d) Mode4.

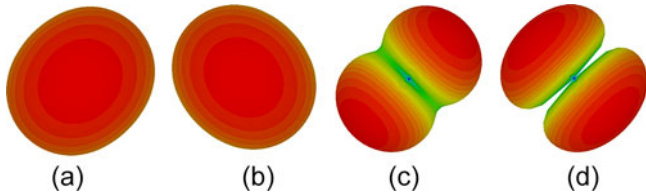


Figure 5. Far field. (a) Mode1. (b) Mode2. (c) Mode3. (d) Mode4.

$$\left| \frac{\Delta S}{S} \right| = \frac{1}{2Q_0} \tag{4}$$

$$S = (Lp1)^2 \tag{5}$$

$$\Delta S = \frac{1}{2}(T1)^2 \tag{6}$$

where  $\Delta S$  represents the area of the corner-cutting,  $S$  represents the area of the patch, and  $Q_0$  is the total quality factor of the antenna, which can be calculated using the following formula [25]:

$$\frac{1}{Q_0} = \frac{1}{Q_r} + \frac{1}{Q_d} + \frac{1}{Q_c} + \frac{1}{Q_{sw}} \tag{7}$$

$$Q_r = \frac{\epsilon_r ab}{60\lambda_0 h \delta_{om} \delta_{on} G_r} \tag{8}$$

$$Q_d = \frac{1}{\tan \delta} \tag{9}$$

$$Q_c = h\sqrt{u_0 \pi f_r \sigma} = \pi h\sqrt{120\sigma/\lambda_0} \tag{10}$$

$$Q_{sw} = \frac{1}{3.4\sqrt{\epsilon_r - 1} \frac{h}{\lambda_0}} Q_r \tag{11}$$

where  $Q_r$ ,  $Q_d$ ,  $Q_c$ , and  $Q_{sw}$  represent the quality factors of radiation, medium, dielectric loss, and surface wave, respectively.  $a$  and  $b$  represent the length and width of the antenna, respectively.  $\sigma$  represents the electrical conductivity of the patch metal.  $\tan \delta$  represents the tangent of the dielectric loss.  $\mu_0$  is the magnetic permeability of vacuum.

If  $G_r \approx 2G_s \approx (a/\lambda_0)^2/45$ , then  $Q_r \approx \frac{3\epsilon_r b/a}{8(h/\lambda_0)}$ . According to the above method, the corner-cutting size  $T1 \approx 1.2$  mm can be preliminarily determined.

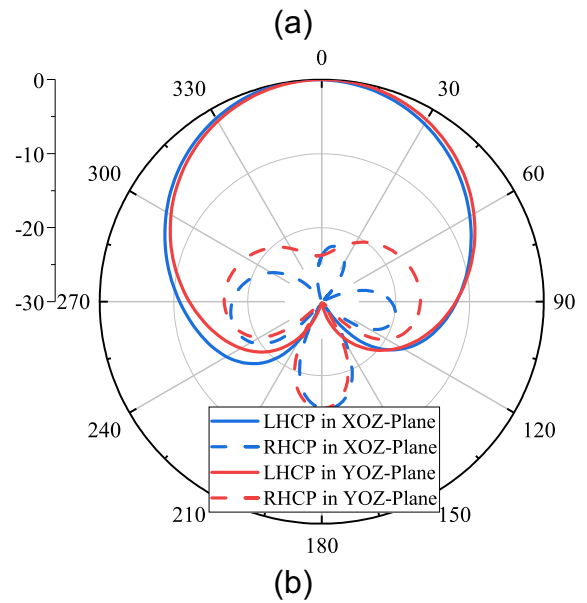
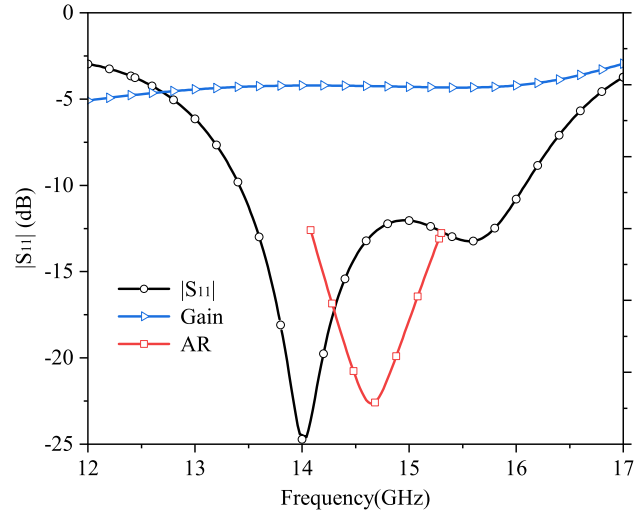
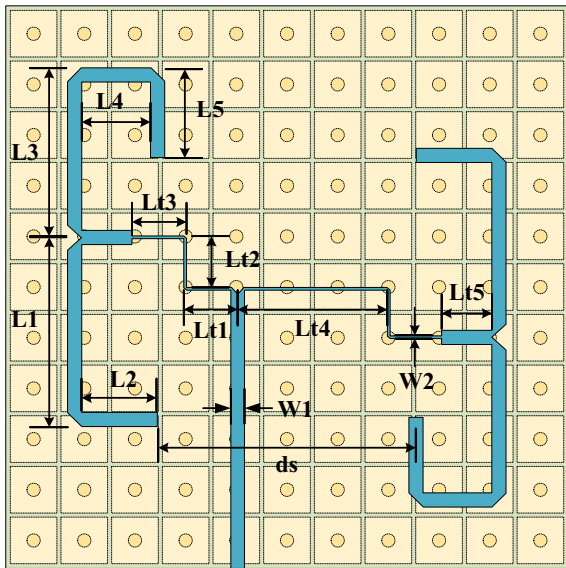


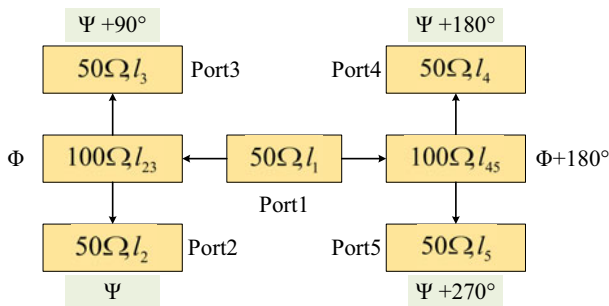
Figure 6. The simulated results of Ant1. (a)  $|S_{11}|$ , gain, and AR. (b) Radiation pattern at 14.7 GHz.

In order to provide a clear physical mechanism, characteristic mode theory is applied to analyze CP characteristics of the antenna element. It provides several important characteristic parameters: eigenvalue ( $\lambda$ ), modal significance (MS), and characteristic angle (CA). The relevant calculation formulas are as follows [26]:





(a)



(b)

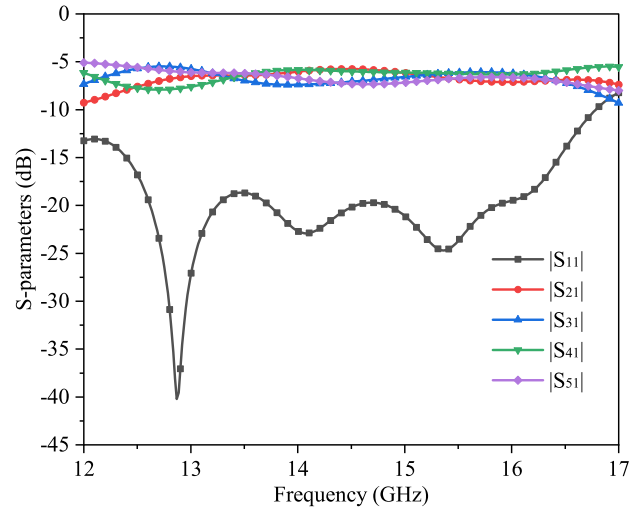
**Figure 7.** (a) SIGW-SRP structure. (b) SRP equivalent circuit. The relevant parameters of SRP feeding network are:  $W1 = 0.8$ ,  $Lt1 = 3$ ,  $Lt2 = 2.85$ ,  $Lt3 = 3$ ,  $Lt4 = 8.55$ ,  $Lt5 = 2.8$ ,  $L1 = 10.5$ ,  $L2 = 5$ ,  $L3 = 9.5$ ,  $L4 = 5.4$ ,  $L5 = 5$ ,  $ds = 14.6$  (units: mm).

$$MS = \left| \frac{1}{1 + j\lambda_n} \right| \tag{12}$$

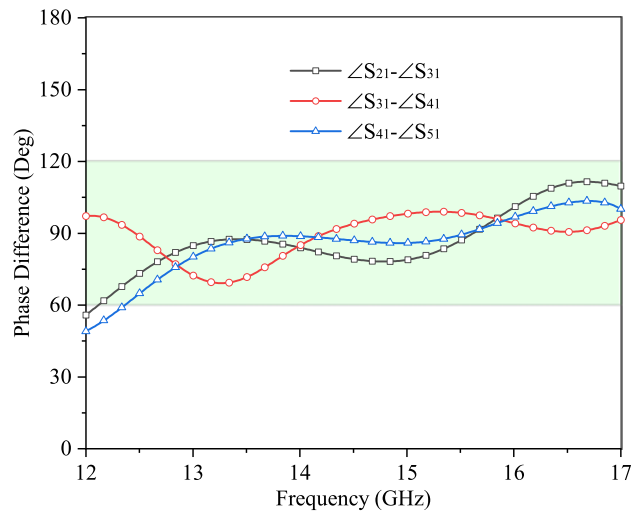
$$CA = 180^\circ - \tan^{-1}\lambda_n \tag{13}$$

where  $\lambda_n$  is the eigenvalue of Mode  $n$ . MS can intuitively show the possible characteristic patterns in the conductor structure. It indicates the contribution of each characteristic mode to the total field. When MS approaches 1, the mode is more likely to resonate easily. When MS approaches 0, the mode is less likely to resonate. Additionally, when  $MS \geq 0.707$ , it is referred to as a significant mode, indicating that the mode is more easily excited. CA is the phase lag between the real characteristic current on the conductor surface and the tangential electric field. When the phase lag is  $180^\circ$ , the corresponding mode is referred to as the most efficient radiating mode [27]. For CP radiation, it is necessary to excite at least two characteristic modes simultaneously. These modes should have  $\lambda$  equal to 0, equal MS values that are all greater than 0.707, and the phase difference between their CA close to  $90^\circ$  [28].

The antenna element without excitation is analyzed using CST software. MS of the first four modes are shown in Fig. 3(a). Mode1 to Mode4 are resonant around at 14.6 GHz, 16.9 GHz, 16.5 GHz, and 16.7 GHz, respectively. Moreover, Mode1 and Mode2 have



(a)



(b)

**Figure 8.** Simulated results of each port of SIGW-SRP. (a) S-parameter curves. (b) The phase difference curves.

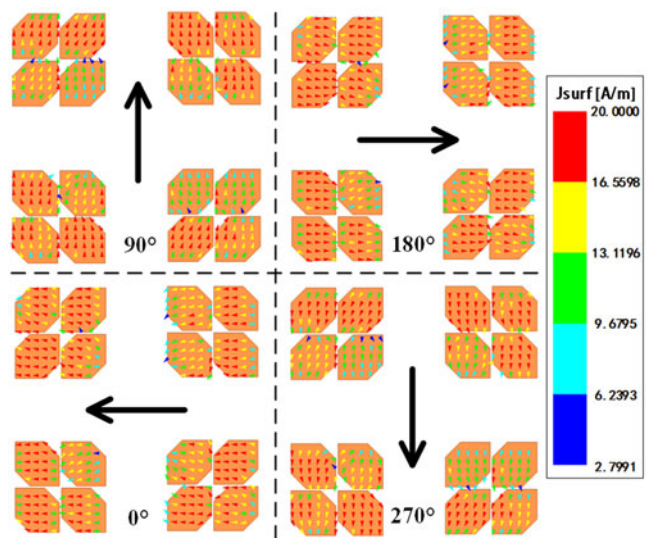


**Figure 9.** Current distribution of the array antenna at 15 GHz.

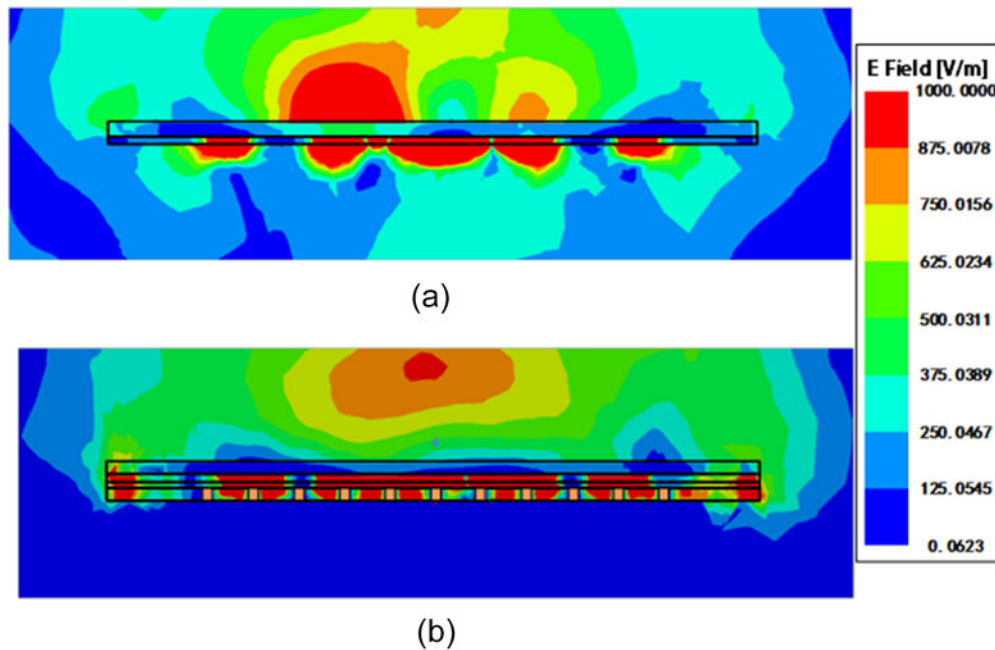


**Figure 10.** Electric field distribution of the array antenna at 15 GHz. (a) Without SIGW. (b) With SIGW.

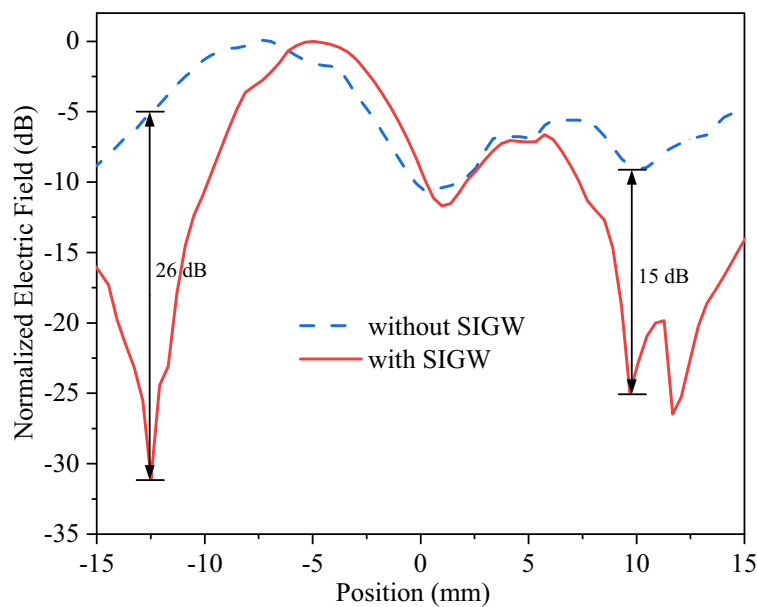


**Figure 11.** Effect of SIGW on transverse electric field distributions.

equal MS at around 15.8 GHz and a phase difference of about  $90^\circ$  in Fig. 3(b). Therefore, the antenna element can produce CP radiation near 15.8 GHz.

To further characterize the radiation performance of the antenna element, the current distributions and radiation patterns of the first four modes at their respective resonance frequencies are shown in Figs. 4 and 5, respectively. Mode1 and Mode2 both exhibit co-directional currents and have orthogonal distributions, indicating that they are a pair of degenerate modes. It is worth mentioning that if the characteristic modes excite counter-directional currents, it can result in radiation cancellation, leading to no radiation energy in the radiation direction. This is evident in the cases of Mode3 and Mode4.

Next, the antenna element is simulated using ANSYS HFSS. From Fig. 6(a), it can be observed that IBW ranges from 13.41 to 16.08 GHz, ARBW ranges from 14.37 to 16.95 GHz, and the gain is greater than 9 dBic. Figure 6(b) shows the radiation pattern at 14.7 GHz in the XOY and YOZ planes, which has greater the left-hand circular polarization (LHCP) gain.

It is worth noting that CP resonance point obtained from CMA is at 15.8 GHz, while the actual simulated CP resonance point is at 14.7 GHz. Due to the aperture coupling feeding used, the resonance generated by the slot can introduce some interference to the antenna's own resonance, thereby causing a deviation in CP resonance point.

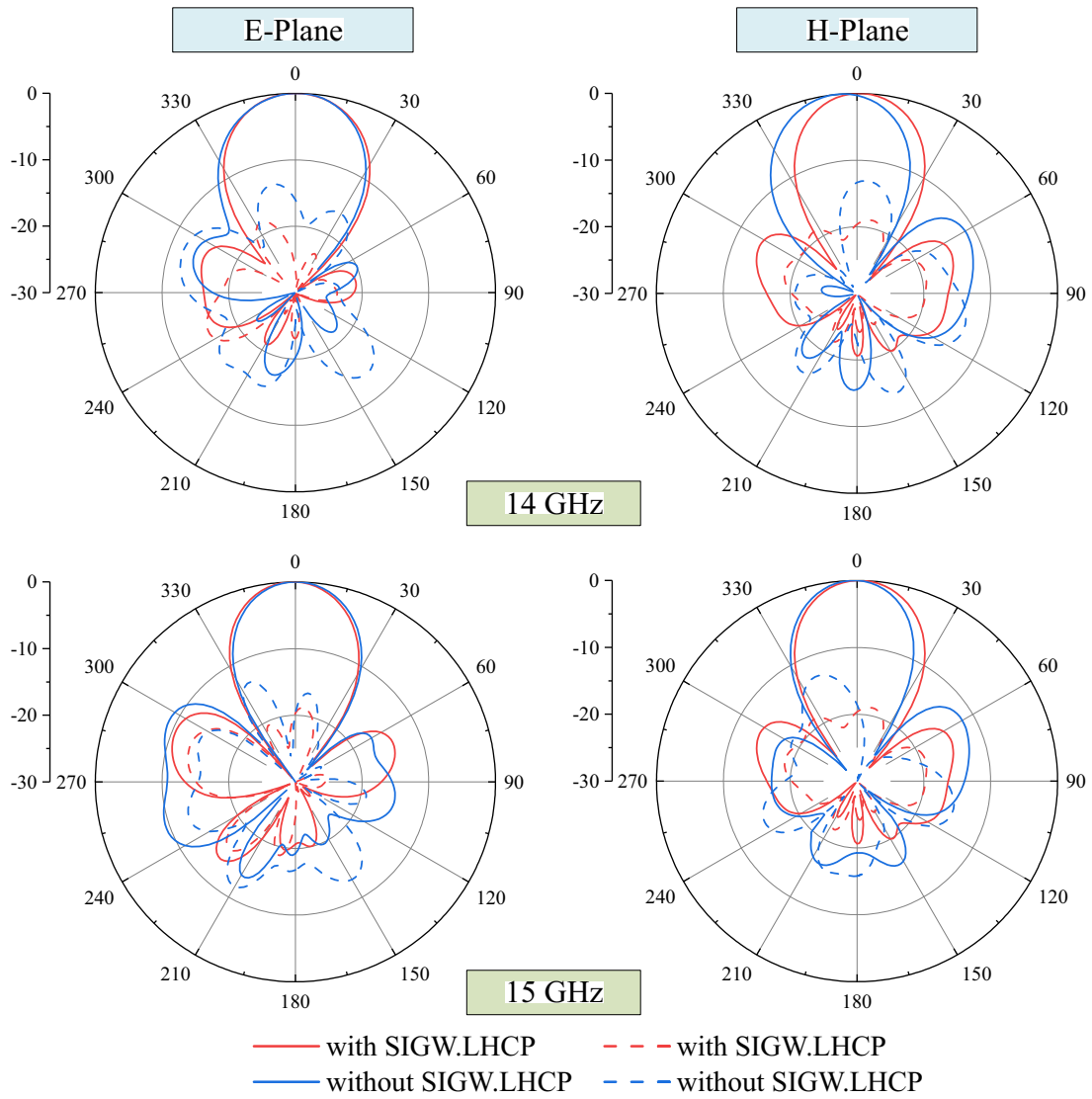


Figure 12. Comparison of simulated radiation patterns with and without SIGW at 14 GHz and 15 GHz.

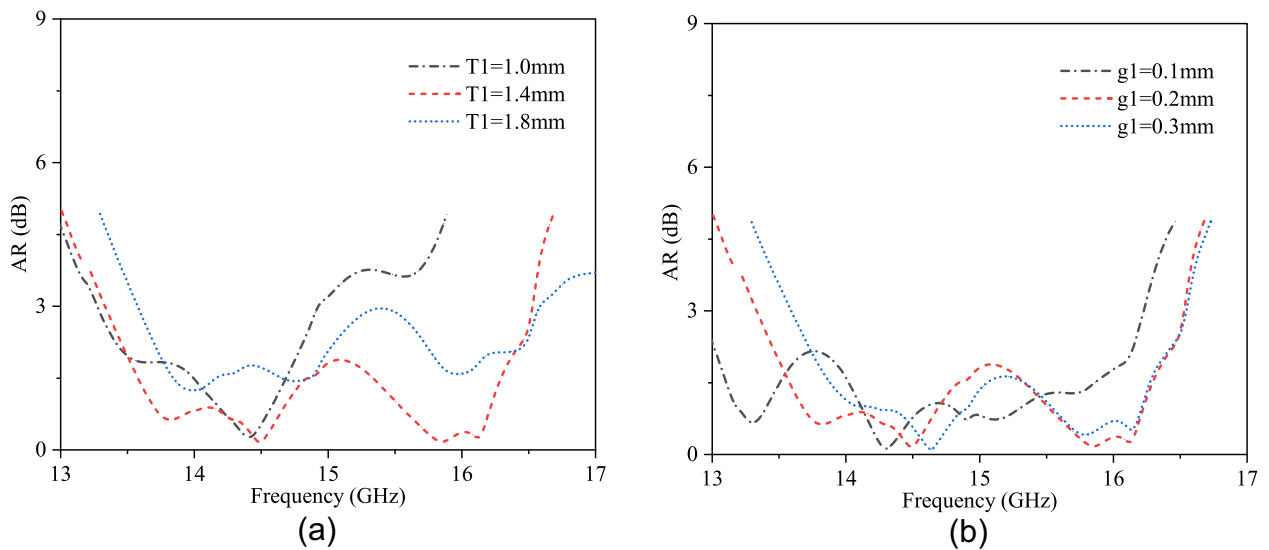
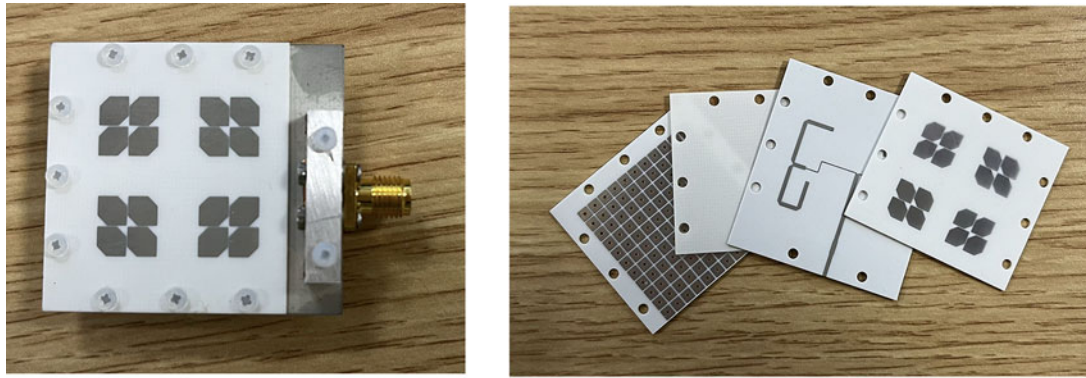
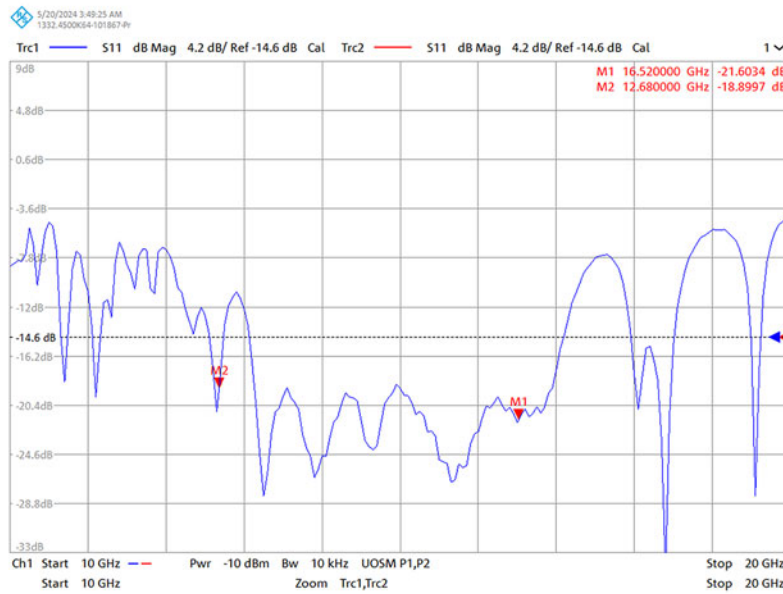


Figure 13. AR under different parameters. (a) T1. (b) G1.



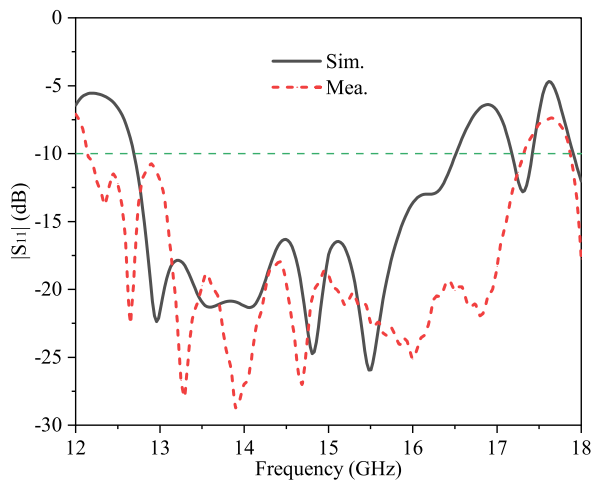
(a)

(b)

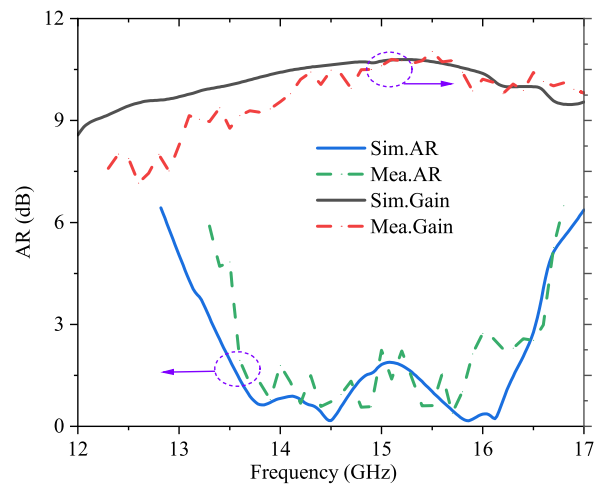


(c)

**Figure 14.** (a) Overall prototype photo of the proposed array antenna. (b) Disassembly prototype photo of the proposed array antenna. (c) The VNA screenshots of S-parameters outcomes.



(a)



(b)

**Figure 15.** The simulated and measured results of Array1. (a)  $|S_{11}|$  and gain. (b) AR.



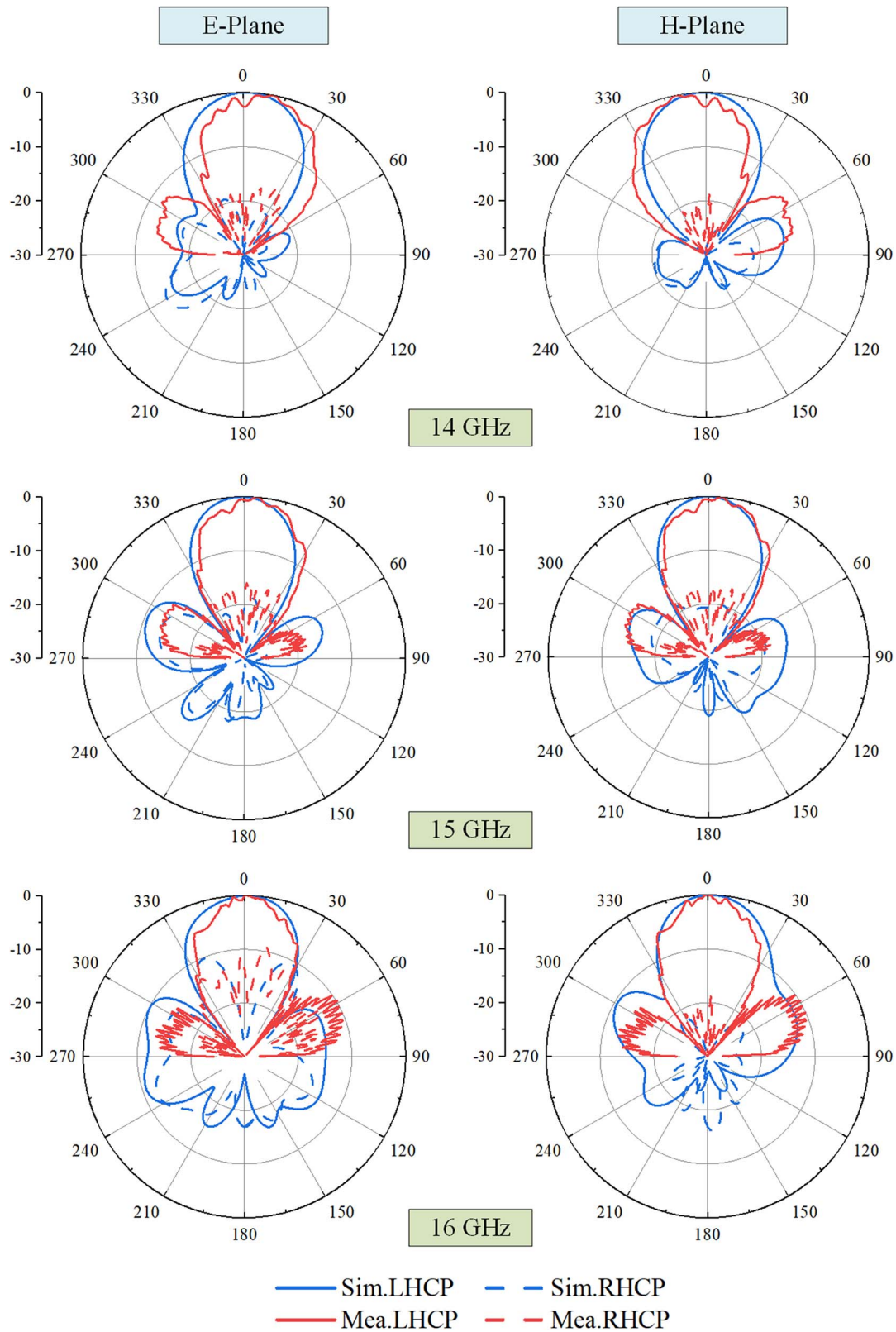


Figure 16. The simulated and measured radiation patterns at 14 GHz, 15 GHz, and 16 GHz.

**Feeding network structure design based SIGW**

The feeding network structure based on SIGW-SRP is shown in Fig. 7(a). The essence of SRP is to optimize the radiation

performance of an antenna by utilizing the vector addition of electromagnetic waves and compensating for phase variations by changing the antenna position. According to characteristic mode

**Table 1.** Comparison to the recently reported CP array antennas based on SRP.

| Ref.      | year | $f_0$ (GHz) | Element num. | IBW (%) | ARBW (%) | Peak gain (dBic) | Size ( $\lambda_0^3$ )          |
|-----------|------|-------------|--------------|---------|----------|------------------|---------------------------------|
| [17]      | 2023 | 14.6        | $2 \times 2$ | 44      | 34.6     | 11               | $1.89 \times 1.65 \times 0.11$  |
| [18]      | 2023 | 5           | $2 \times 2$ | 38      | 24.9     | 12.1             | $2.18 \times 2.18 \times 0.06$  |
| [29]      | 2022 | 10          | $2 \times 2$ | 21      | 18       | 13.2             | $3.7 \times 3.7 \times 0.11$    |
| [30]      | 2023 | 6           | $2 \times 2$ | 37.3    | 22.5     | 13               | $1.81 \times 1.81 \times 0.05$  |
| [31]      | 2024 | 28          | $2 \times 2$ | 41.6    | 16.6     | 13.9             | $2.02 \times 1.74 \times 0.17$  |
| [32]      | 2024 | 31          | $2 \times 2$ | 40.7    | 27.4     | 11.1             | $1.46 \times 1.46 \times 0.076$ |
| This work |      | 14.5        | $2 \times 2$ | 34.6    | 21.2     | 16               | $1.5 \times 1.5 \times 0.11$    |

theory, it can be determined that achieving CP characteristics requires a phase difference of  $90^\circ$ . Therefore, by sequentially delaying the output energy of each port of the feeding network by  $90^\circ$ , the array antenna can exhibit different CP resonance characteristics to expand bandwidth [18].

To demonstrate the working mechanism of the feeding network, the equivalent circuit of SRP is shown in Fig. 7(b). Equal power distribution among the ports of the feeding network is achieved by varying the widths of the branches. Furthermore, the desired sequential rotation of phase by  $90^\circ$  for each port is achieved by adjusting the lengths of the branches. Due to equal power distribution is desired among the ports, the following can be obtained:

$$P_2 = P_3 = P_4 = P_5 = \frac{P_1}{4} \quad (14)$$

$$l_3 = l_2 + l_{\lambda/4} \quad (15)$$

$$l_5 = l_4 + l_{\lambda/4} \quad (16)$$

$$l_{45} = l_{23} + l_{\lambda/2} \quad (17)$$

where  $P_n$  represents the power at each port and  $l_n$  represents the electrical length of each branch ( $n = 1, 2, \dots$ ).

From Fig. 8(a), it can be observed that S-parameter curves of all ports in the SRP feeding network. Within the range of 12.5–16.5 GHz,  $|S_{11}|$  is consistently less than  $-15$  dB, and  $|S_{21}|$  to  $|S_{51}|$  are all within the range of  $-6 \pm 2$  dB. Additionally, from the phase difference curves of adjacent ports in Fig. 8(b), it can be observed that within the range of 12.5–16.5 GHz, the phase difference between adjacent ports remains within  $90^\circ \pm 30^\circ$ . Since SIGW can achieve a wide and stable IBW, the SIGW-SRP feeding network achieves the wide bandwidth and stable phase difference curves [19].

In summary, the design procedures of the proposed antenna are as follows:

- (1) The SIGW structure is designed to operate in the Ku-band to reduce back radiation and surface wave leakage.
- (2) The size of the antenna element corner-cutting is calculated by theoretical formula. Characteristic mode analysis method is used to guide the antenna element design, and the first two modes (a pair of degenerate modes) are selected as the operating modes to achieve wide IBW and generate CP waves.
- (3) The SIGW-SRP feed network is designed with a phase difference of  $90^\circ$  between two adjacent ports. By utilizing spatial

vector superposition, the axial bandwidth is further expanded, and the gain is improved.

- (4) The antenna element and the SIGW-SRP feeding structure are designed in combination to finally form a  $2 \times 2$  array antenna.

### Verification and analysis

Figure 9 shows the current distribution of the proposed array antenna at 15 GHz, and the current flows in the clockwise direction at  $0^\circ$ ,  $90^\circ$ ,  $180^\circ$ , and  $270^\circ$  phases, explaining the left-hand circular polarization (LHRP) operation mechanism.

To further illustrate the advantages of SIGW, the antenna with SIGW and the antenna without SIGW are simulated respectively. Figure 10 shows the electric field distribution observed on a reference plane. It can be seen that the antenna loaded with SIGW has almost no back radiation compared to the antenna without SIGW loading. Figure 11 shows the transverse electric field distribution on a reference line, where loading SIGW reduces the edge electric field by 26 dB and 15 dB on both sides, respectively, proving that loading SIGW can significantly suppress the transverse radiation. At the midpoint, both curves have a slight decrease because there is no radiating element in the center of the array antenna. The above simulation results show that loading SIGW can suppress the back radiation and transverse radiation, which is because SIGW can achieve in-phase reflection and suppress surface wave leakage at the high frequency band [22]. Figure 12 shows the radiation pattern of the two antennas at 14 GHz and 15 GHz. It can be seen that the antenna loading SIGW has an average backlobe reduction of about 3.8 dB in the  $180^\circ$  direction and an average cross-polarization reduction of about 4.6 dB in the  $0^\circ$  direction, which proves the effect of SIGW to suppress the back radiation to improve directivity and suppress the cross polarization.

To improve the circular polarization performance, parameter analyses are conducted. As shown in Fig. 13, both the corner-cutting size of the antenna element and the spacing between the patches affect the circular polarization characteristics, with the corner-cutting size having a more significant impact.

To validate the performance of the proposed array antenna, a prototype is fabricated. The prototype photos and the vector network analyzer (VNA) screenshots are shown in Fig. 14. As seen from Fig. 15(a), the measured  $-10$  dB IBW is from 12.2 to 17.3 GHz (34.6%), while the simulated one is from 12.4 to 16.4 GHz (27.8%). As seen from Fig. 15(b), the measured 3 dB ARBW ranges from 13.5 to 16.7 GHz (21.2%), while the simulated one ranges from 13.3 to 16.5 GHz (21.5%), and the measured peak gain is 16 dBic, while the simulated peak gain is 16.1 dBic. It is worth noting that due to factors such as processing accuracy, measuring, and the connector,

there are some deviations between the measured results and the simulated results.

Figure 16 shows the radiation patterns of the proposed array antenna at different frequencies. It can be observed that the proposed array antenna is LHCP with good symmetry. In addition, from the electric field distribution in Fig. 10, it can be well explained that the proposed array antenna can suppress the cross-polarization of about 17 dB at the 0° axial radiation direction due to the use of SIGW.

In order to further describe the performance of the proposed array antenna, some recently reported SRP array antennas are listed in Table 1. Compared with [17, 18, 30] and [32], although the proposed array antenna has a narrower bandwidth, it has higher gain. Overall, the proposed array antenna has obvious advantages in size and gain, which aligns with the trend toward miniaturization development.

## Conclusion

A compact, wideband, and high-gain CP array antenna based on SIGW-SRP feeding network is proposed in this paper. Due to the antenna element can only achieve narrow bandwidth and low gain, a  $2 \times 2$  array antenna is achieved through the compensation phase of the SIGW-SRP feeding network, which can greatly expand the bandwidth and improve the gain. The measured results show that the  $-10$ -dB IBW of the antenna is from 12.2 to 17.3 GHz (34.6%), the 3-dB ARBW is from 13.5 to 16.7 GHz (21.2%), and the peak gain reaches 16 dBic. Simulation results show that loading SIGW can reduce the back radiation and transverse radiation. The proposed antenna achieves broadband, high gain, and compact size, making it suitable for space-limited communication applications.

**Acknowledgements.** This research is supported by the National key research and development program of China (No2021YFB2900401) and State Key Laboratory of Matamaterial Electromagnetic Modulation Technology (Research on Low RCS Reconfigurable Antenna based on electromagnetic metamaterials).

**Competing interests.** The author(s) declare none.

## References

- Bertrand M, Ettorre M, Valerio G, Albani M and Casaletti M (2023) A broadband low-profile circularly polarized radial line slot antenna. *IEEE Transactions on Antennas and Propagation* **71**, 140–150.
- Ding X, Zhao Z, Yang Y, Nie Z and Liu QH (2018) A compact unidirectional ultra-wideband circularly polarized antenna based on crossed tapered slot radiation elements. *IEEE Transactions on Antennas and Propagation* **66**, 7353–7358.
- Kun C, Li Z, Zhao Y, Han L, Han G and Liu Y (2023) A low-profile wideband circularly polarized metasurface antenna based on characteristic mode analysis. *International Journal of Microwave and Wireless Technologies* **7**, 1–8.
- Birwal A, Patel K and Singh S (2024) Circular slot-based microstrip circularly polarized antenna for 2.45-GHz RFID reader applications. *IEEE Journal of Radio Frequency Identification* **8**, 10–18.
- Han G, Zheng Z, Su J, Yuan H and Zhang W (2024) Wideband nonuniform metasurface antenna with stable gain. *International Journal of Microwave and Wireless Technologies* **16**, 268–275.
- Wei X, He L, Zeng J, Fei D and Liu H (2023) A center-fed triple-mode wideband circularly polarized phased array using characteristic-mode analysis. *IEEE Antennas and Wireless Propagation Letters* **22**, 1677–1681.
- Li W, Xue W, Li Y, Chung K and Huang Z (2023) A wideband differentially fed circularly polarized slotted patch antenna with a large beamwidth. *Journal of Electromagnetic Engineering and Science* **23**, 512–520.
- Cheng G, Zhou J, Yang L, Wu X and Huang Z (2023) A stacked circularly polarized filtering antenna with crossed slot. *IEEE Antennas and Wireless Propagation Letters* **22**, 2935–2939.
- Muntoni G, Casula G, Traversari M and Montisci G (2024) A wideband single-feed circularly polarized stacked patch antenna. *IEEE Access* **12**, 103380–103387.
- Shi T, Chai R, Chen X, Li M, Zhang T and Tang M (2023) A low-profile, circularly polarized, metasurface-based antenna with enhanced bandwidth and stable high gain. *IEEE Antennas and Wireless Propagation Letters* **22**, 253–257.
- Li L, Wu Z, Liang J and Su M (2023) Wideband and low profile multi-polarization reconfigurable antenna based on metasurface. *Microwave and Optical Technology Letters* **65**, 2793–2801.
- Wu J, Yang W, Gu L, Xue Q and Che W (2022) Low-profile wideband dual-circularly polarized metasurface antenna based on traveling-wave sequential feeding mechanism. *IEEE Antennas and Wireless Propagation Letters* **21**, 1085–1089.
- Chen Q, Zhang G, He C, Fan Y, Zhu Z, Zhang D, Li J and Zhao Y (2021) Wideband and high-gain circularly-polarized L-shaped slot antenna array using metamaterial. *International Journal of Microwave and Wireless Technologies* **13**, 359–364.
- Cheng G, Huang B, Huang Z and Yang L (2023) A high-gain circularly polarized filtering stacked patch antenna. *IEEE Antennas and Wireless Propagation Letters* **22**, 995–999.
- Yousfi A, Lamkaddem A, Abdalmalak K and Segovia-Vargas D (2023) A broadband circularly polarized single-layer metasurface antenna using characteristic-mode analysis. *IEEE Transactions on Antennas and Propagation* **71**, 3114–3122.
- Ma C, Ma Z-H and Zhang X (2019) Millimeter-wave circularly polarized array antenna using substrate-integrated gap waveguide sequentially rotating phase feed. *IEEE Antennas and Wireless Propagation Letters* **18**, 1124–1128.
- Liu H, Zhang Y and Zhao X (2023) A ku wideband circularly polarized microstrip antenna array with low profile crossed-dipole element. *International Journal of Antennas and Propagation* **2023**, 1–10.
- Bai H, Wang G and Zou X (2023) High gain and circularly polarized substrate integrated waveguide cavity antenna array based on metasurface. *Chinese Physics B* **32**, 014101.
- Zhang J, Zhang X and Kishk AA (2018) Broadband 60 GHz antennas fed by substrate integrated gap waveguides. *IEEE Transactions on Antennas and Propagation* **66**, 3261–3270.
- Attia H, Sorkherizi MS and Kishk AA (2015) 60 GHz slot antenna array based on ridge gap waveguide technology enhanced with dielectric superstrate. In *2015 9th European Conference on Antennas and Propagation (EuCAP)*, Lisbon, Portugal: IEEE, pp. 1–4.
- Lin Q, Shen D, Wang L and Luo Z (2024) An mmWave dual-band integrated substrate gap waveguide single cavity filter with frequency selectivity. *China Communications* **21**, 188–199.
- Wang L, Shen D, Lin Q, Luo Z, Wang W, Chen J, Gao Z and Zhang W (2024) An ISGW filtering antenna with spurious modes and surface wave suppression for millimeter wave communications. *China Communications* **20**, 1–12.
- Bayat-Makou N and Kishk AA (2017) Millimeter-wave substrate integrated dual level gap waveguide horn antenna. *IEEE Transactions on Antennas and Propagation* **65**, 6847–6855.
- Han J, Shen D, Cao X, Gao J, Wei J, Zhao Y, Li S and Zhang Z (2018) Broadband radar cross section reduction using dual-circular polarization diffusion metasurface. *IEEE Antennas and Wireless Propagation Letters* **17**, 969–973.
- Wang Z, Fang S, Wang Q and Liu H (2012) An ANN-based synthesis model for the single-feed circularly-polarized square microstrip antenna with truncated corners. *IEEE Transactions on Antennas and Propagation* **60**, 5989–5992.

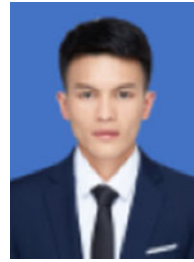
26. **Li L, Wu Z, Liang J and Su M** (2023) Wideband and low profile multi-polarization reconfigurable antenna based on metasurface. *Microwave and Optical Technology Letters* **65**, 2793–2801.
27. **Garbacz RJ** (1965). Modal expansions for resonance scattering phenomena. *Proceedings of the IEEE* **53**, 856–864.
28. **Chen Y and Wang C** (2012) Characteristic-mode-based improvement of circularly polarized U-slot and E-shaped patch antennas. *IEEE Antennas and Wireless Propagation Letters* **11**, 1474–1477.
29. **Wang W, Jin H, Yu W, Zhang XH, Chin K-S and Luo GQ** (2022) A wideband circularly polarized  $2 \times 2$  filtenna array with multiple radiation nulls. *IEEE Antennas and Wireless Propagation Letters* **21**, 595–599.
30. **Pramono S, Sumantyo J, Ibrahim M, Takahashi A, Yoshimoto Y, Kashiwara H, Santosa C, Gao S and Ito K** (2023) Circularly polarized lunar regolith simulant antenna for future communication and remote sensing in lunar environment. *IEEE Antennas and Wireless Propagation Letters* **22**, 2988–2992.
31. **Xie Y, Zhao J, Sun Y and Xu J** (2024) A broadband circularly polarized antenna for millimeter-wave applications. *International Journal of Microwave and Wireless Technologies* **14**, 1–8.
32. **Ye J, Li T, Han M and Dou W** (2024) Metasurface-inspired wideband circularly polarized antenna array in Ka-band using characteristic mode analysis. *IEEE Antennas and Wireless Propagation Letters* **23**, 389–393.



**Pengpeng Chen** received the B.S. degree in Measurement and Control Technology and Instrument from Wuhan University (WHU) in 2021. He is currently pursuing the master degree at school of electronics and communication engineering, Sun Yat-sen University (SYSU). His current research is wideband circularly polarized metamaterial antenna.



**Wenjian Wang** received the M.S. degree in Environmental Chemistry from Fuzhou University, Fuzhou, Fujian, China, in 2010. Since then, he has been joined Kuang-Chi Institute of Advanced Technology China, where he was a researcher on electronic engineering. He is currently pursuing the Ph.D. degree with the College of Electronics and Communication Engineering, Sun Yat-sen University, Shenzhen, China. His current research interests include metamaterials, high-gain antenna arrays, radar, RCS reduction, ultrawideband technology, and wave propagation in complex media.



**Lihui Wang** received the M.S. degree in communication and information system from Yunnan University, Kunming, China, in 2022, and he is currently pursuing the Ph.D. degree at the school of electronics and communication engineering, Sun Yat-sen University, Shenzhen, China. His current research interests include phased array antenna technology and millimeter antenna for satellite communications.



**Qihua Lin** received the B.S. degree, in 2018. And he received the M.E. degree from Yunnan University, Kunming, China, in 2022. He is currently pursuing the Ph.D. degree at Sun Yat-sen University, Shenzhen, China. His current research interests include communication, electronic information, and other related professional fields, including theoretical and design research.



**Da Hou** received the B.S. degree from the Changsha University of Science and Technology, Changsha, China, in 2020, the M.S. degree in communications and information systems from the Yun University, Kunming, China, in 2023. He is currently a joint Ph.D. student at Sun Yat-sen University and Pengcheng Laboratory. His current research interests include computational electromagnetics, microwave sensors, frequency selectivity surface, and filtering antenna.



**Zhiyong Luo** He is currently a Professor at the school of electronics and communication engineering, Sun Yat-sen University, Shenzhen, China. He received Ph.D. from the University of Electronic Science and Technology, Chengdu, China, in 2000. He participated in national key national defense plans such as 995/810/934. His research interests include communication, electronic information, and network.